CFD Letters

Journal homepage:
https://semarakilmu.com.my/journals/index.php/CFD_Letters/index
ISSN: 2180-1363

Numerical Investigation on Photovoltaic Thermal Panel using Various Nanofluids Concentrations

Cheah Kai Xiang[1], Mohd Afzanizam Mohd Rosli[1,*], Probowo[2], Safarudin Gazali Herawan[3], Mohamed Teggar[4], Nona Merry M. Mitan[5]

[1] Faculty of Mechanical Technology and Engineering, Universiti Teknikal Malaysia Melaka, Hang Tuah Jaya, 76100 Durian Tunggal, Melaka, Malaysia
[2] Departemen Teknik Mesin ITS, Gedung C Lantai II, Kampus ITS Sukolilo, Surabaya 60111, Indonesia
[3] Industrial Engineering Department, Faculty of Engineering, Bina Nusantara University, Jakarta, Indonesia
[4] Laboratory of Mechanics, University of Laghouat, 03000, Algeria
[5] Chemistry Department, Universitas Pertamina, Jl. Teuku Nyak Arief, Simprug, Kebayoran Lama, Jakarta 12220, Indonesia

ARTICLE INFO

Article history:
Received 27 June 2024
Received in revised form 21 July 2024
Accepted 19 August 2024
Available online 31 October 2024

Keywords:
Photovoltaic Thermal System (PVT); Computational Fluid Dynamic (CFD); nanofluid; thermal efficiency; electrical efficiency

ABSTRACT

Increasing the efficiency of solar panels is crucial for effective use of renewables. The present numerical study deals with improving the performance of a PVT system with nanofluid using CFD FLUENT software. ZnO-water and SiO_2-water nanofluids are investigated and correlation are established between the PVT efficiency and various nanofluid volumetric concentrations ranging from 1% to 10%. Validation of the present results is verified by comparison with experimental data. Comprehensive research is conducted to evaluate the correlation between the thermophysical properties of nanofluids such as density, thermal conductivity, specific heat capacity and dynamic viscosity. The results demonstrate that the overall efficiency of the ZnO-water nanofluid and SiO_2-water nanofluid increases by 0.44% and 0.24%, respectively, as the volumetric concentration of the nanofluid rises from 1% to 10%. The ZnO-water nanofluid reveals enhanced thermal and electrical efficiency compared to the SiO_2-water nanofluid due to its superior thermal conductivity and enhanced heat transfer capabilities along the absorber tube. The ZnO-water nanofluid exhibits a greater heat transfer coefficient, thereby facilitating the cooling mechanism of the PV panel and reducing the PV cell temperature, hence enhancing power generation.

1. Introduction

The increasing global energy demand resulting from population growth and living standard, coupled with the negative environmental effects of fossil fuels, has forced the utilisation of various technologies that use renewable energy and convert the energy into electricity. Therefore, global demand and enthusiasm for renewable energy from alternative sources have been on a steady rise in recent decades [1]. The photovoltaic-thermal (PVT) system utilises solar energy via the photovoltaic effect to generate electricity, while at the same time utilising the waste heat produced

* *Corresponding author.*
E-mail address: afzanizam@utem.edu.my (Mohd Afzanizam Mohd Rosli)

https://doi.org/10.37934/cfdl.17.4.6688

by the PV panels for thermal applications [2]. PVT systems enable both the capabilities of solar energy collection and concurrent generation of electrical and thermal energy within a single system [3].

Addition of nanoparticles to the PVT system's cooling base fluid can enhance the system's effectiveness for both laminar and turbulent flow [4]. Nanofluids are defined as colloidal suspensions comprising nanoparticles that are suspended in a base fluid. The concept of nanofluids was first proposed by Choi SUS and Eastman JA in 1995 [5]. Nanofluids feature increased thermal conductivity and heat transfer coefficients, which assist in convective heat transfer from photovoltaic panels to the moving fluid. The theory behind the enhancement of thermal conductivity and heat transfer capabilities is attributed to the suspension of solid particles within the energy transmission fluids. The nanoparticles can reduce the thickness of the boundary layer of the fluid, thereby facilitating convective heat transfer and strengthening the heat dissipation process. The characteristic of nanofluids helps to mitigate the risk of overheating and potential thermal degradation of the PV cells.

Etminan-Farooji *et al.,* [6] reported that the utilisation of nanofluids, such as Al_2O_3-water and CuO-water nanofluids, has exhibited superior heat transfer capabilities compared to pure water and various base fluids. In order to assess the effects of adding SiO_2 nanoparticles to the water-based operating fluid of a sheet and tube PVT system, Sardarabadi *et al.,* [7] conducted an experimental study on the evaluation of the PVT performance and thermal efficiencies utilises the first and second laws of thermodynamics. The outcomes of the study reveal that the overall energy efficiency is enhanced by 3.6% and 7.9% for nanofluids containing 1 wt% and 3 wt%, respectively. Radwan *et al.,* [8] used Al_2O_3-water nanofluids to investigate the effects of microchannel cooling on PV cells in laminar flow conditions. The results indicated that the nanofluid outperformed water in PV panel cooling processes, especially at fluid flows with low Reynolds numbers. Said *et al.,* [9] carried out an experimental investigation to assess the heat transmission of nanofluid in flat plate solar collectors. The experiment incorporates Al_2O_3 nanoparticles' density, thermal conductivity, and viscosity into the pressure drop and the electrical power generated by using water and ethylene glycol/water as base fluids. It was discovered that the thermal conductivity of nanofluids is significantly greater than base fluids, and the viscosity of nanofluids is dependent on the temperature and volume concentration of the fluids.

Al-Waeli *et al.,* [10] executed a numerical analysis for evaluating the impact of various types of nanoparticles namely SiC, CuO, Al_2O_3 , and base fluids including water, glycerin, and ethylene glycol on the performance of convection heat transfer in PVT systems. The outcomes point out that both the convective transfer of heat and the pressure drop were influenced by the thermophysical properties of both the base fluid and nanoparticles. The convective heat transfer performance of SiC nanofluids was found to be superior to that of CuO and Al_2O_3nanofluids. The utilisation of a 3 wt% SiC nanofluid resulted in a notable enhancement in the electrical efficiency of the system by 24.1% and the thermal efficiency by 100.19% in comparison to the utilisation of water as a coolant in PVT systems. Teng *et al.,* [11] investigated the impact of altering the structure size of nanoparticles and the ambient temperature on the thermal transfer rate with the usage of Al_2O_3-water nanofluid in the PVT system. It was determined that the enhancement of temperature and reduction in the nanoparticles size would end up resulting in an improvement in thermal conductivity.

An analysis of the performance evaluation of a nanofluid-based PVT system involving Al_2O_3-water nanofluid and Ag-water nanofluid at various concentrations (0% to 12%) was carried out numerically by Khanjari *et al.,* [12]. It was shown that the thermal and electrical efficiency of the PVT system rises as the volume fraction of the nanoparticles increases for both nanofluids. Based on the reported result, Ag-water nanofluids demonstrate an overall efficiency improvement of 10.21% in the PV/T system at a volume fraction of 0.12. The data indicates that the enhancement of overall

efficiency at low volumetric concentrations is significant, yet it will gradually stagnate upon reaching an optimal level of volumetric concentration.

Furthermore, Jia *et al.,* [13] conducted a comparative analysis of metal oxide-based nanofluid in a PVT system to assess the influence of nanoparticle thermal conductivity on PVT performance at various volumetric concentrations (0%, 3%, and 6%). The findings of the research indicate that 6% of the nanoparticle volumetric concentrations of Al_2O_3-water and TiO_2-water nanofluids show the greatest electrical and thermal power compared with other volumetric concentrations of both nanofluids. The enhanced thermal conductivity characteristic enables efficient heat transfer within the fluid flow in pipes, leading to higher PVT performance, hence enhancing the production of thermal and electrical power. Table 1 summarises the nanofluid's type and its thermophysical properties in previous research.

Table 1
The type of nanofluid and its thermophysical properties in existing studies

References	Nanoparticle	Type	Volumetric Concentration φ (%)	Density ρ ($\frac{kg}{m^3}$)	Thermal conductivity k ($\frac{W}{mK}$)	Specific heat capacity c_p ($\frac{J}{kgK}$)	Thermal efficiency Enhancement (%)	Electrical efficiency Enhancement (%)
Khanjari *et al.,* [12]	Silver (Ag)	Metal-based	0%~12%	10500	429	235	10	0.21
	Alumina (Al_2O_3)	Metal oxide-based		3970	40	765	3	0.54
Jia *et al.,* [13]	Alumina (Al_2O_3)	Metal oxide-based	0%, 3%, 6%	3970	40	765	-	0.35
	Titanium Oxide (TiO_2)	Metal oxide-based		4250	8.9583	686.2	-	-
Hosseinzadeh *et al.,* [14]	Zinc Oxide (ZnO)	Metal oxide-based	0%~12%	5600	13	495	9.66	0.28
Oztop *et al.,* [15]	Alumina (Al_2O_3)	metal oxide based	0%~3%	3970	40	765	-	-
	Aluminium (Al)	metal based		2719	202.4	871	-	-
Khan *et al.,* 2022 [16]	Iron Oxide (FE_3O_4)	metal oxide based	3%	5180	9.7	670	-	-
	Silicon Dioxide (SiO_2)		3%	2330	36	765	-	-
Mohd Rosli *et al.,* [17]	Multiwalled Carbon Nanotubes (MWCNT)	Carbon nanotubes	0%~1%	1600	3000	796	20.22	0.32
Hasan *et al.,* [18]	Alumina (Al_2O_3)	Metal oxide based	3%	3600	36	765	-	-
	Silicon Dioxide (SiO_2)		3%	2200	1.2	703	-	-
	Copper Oxide (CuO)		3%	6500	20	535.6	-	-
	Zinc Oxide (ZnO)		3%	5600	13	495.2	-	-

2. Methodology

2.1 Geometry Modelling

The present study employs the PVT model, whose geometry is derived from the PVT numerical analysis conducted by Khanjari *et al.,* [12]. The reference model was selected based on its comprehensive simulation data as presented in the research article, which surpasses that of other reference sources. Table 2 specifies the dimensions of the SolidWorks-built PVT models and the imports to the ANSYS Workbench for replicated, simulated, and verified purposes. The components engaged in the CFD simulations involve the glass enclosure, photovoltaic (PV) module, absorber plate, and absorber tube as shown in Figure 1. The PV module is positioned below the glass case, while the absorber plate and absorber tube are located beneath the PV surface.

Table 2
The dimensions of the PVT models

Components	Dimensions (m)	Specification
1. Glass Case	1.6 x 0.3 x 0.002	(Length x Width x Height)
2. PV panels	1.6 x 0.3 x 0.002	(Length x Width x Height)
3. Absorber plate	1.6 x 0.3 x 0.004	(Length x Width x Height)
4. Absorber tube	1.6 x 0.011 x 0.001	(Length x Outer diameter x Thickness)

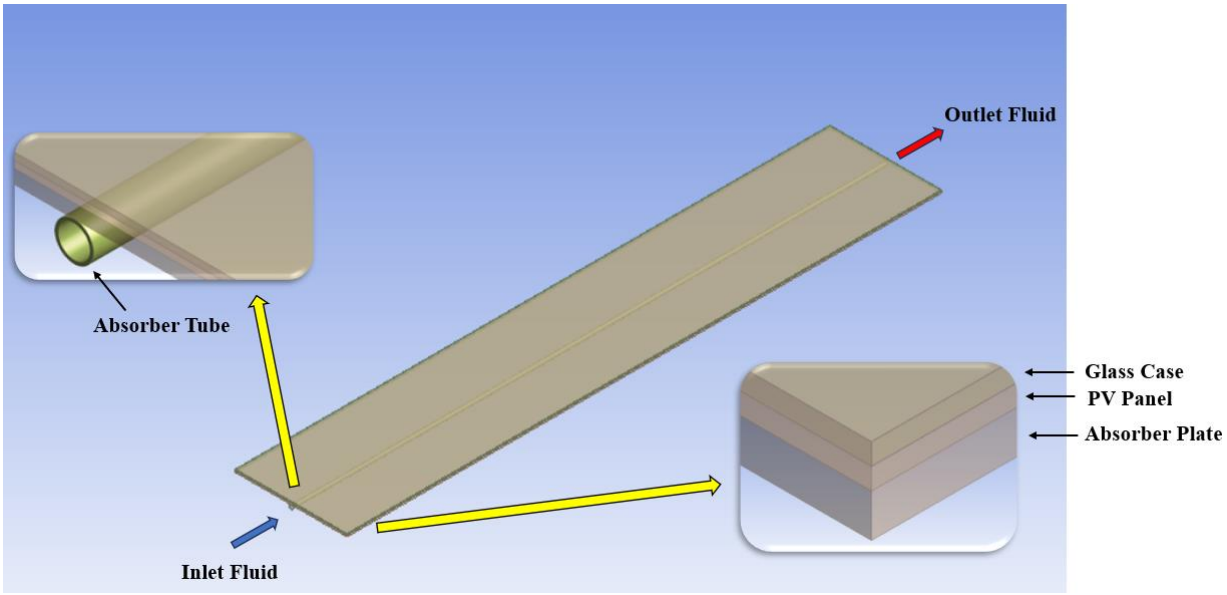

Fig. 1. Schematic diagram of present study PVT model

2.2 Initial and Boundary Conditions

The implemented boundary conditions implemented in present study are as follows, as determined by the research [6]:

i. The PVT system's initial temperature is uniformly set at 30℃
ii. The boundary conditions for the walls are characterized as "no slip" and "impermeable."
iii. The absorbed solar radiation on the absorber plate is calculated via Eq. (1), by taking into consideration the impact of various factors such as the transmissivity of the glass case and the absorptivity of the absorber plate.

iv. The heat flux is subjected perpendicularly to the glass case while the adiabatic boundary conditions are maintained on the opposing side of the absorber plate and the exterior layer of the tube as shown in Figure 2
v. The heat generation rate of the PV cell is equivalent to the absorbed solar radiation.
vi. It is assumed that the heat transfer from the glass surface to the ambient air occurs via conductive, convective, and radiative mechanisms.
vii. The PVT model exhibits distinct interface boundary conditions across its various surfaces and different components.

$$\text{Absorbed Heat Flux} = G_t \tau_g \alpha (1 - \eta) \quad (1)$$

For Eq. (1), $G_t, \tau_g, \alpha, \text{and } \eta$ represent the solar radiation intensity, glass cover transmittivity, glass absorptivity and efficiency, respectively. The boundary conditions are presented as mathematical equations in Table 3, whereas the parameters of the PVT component are detailed in Table 4.

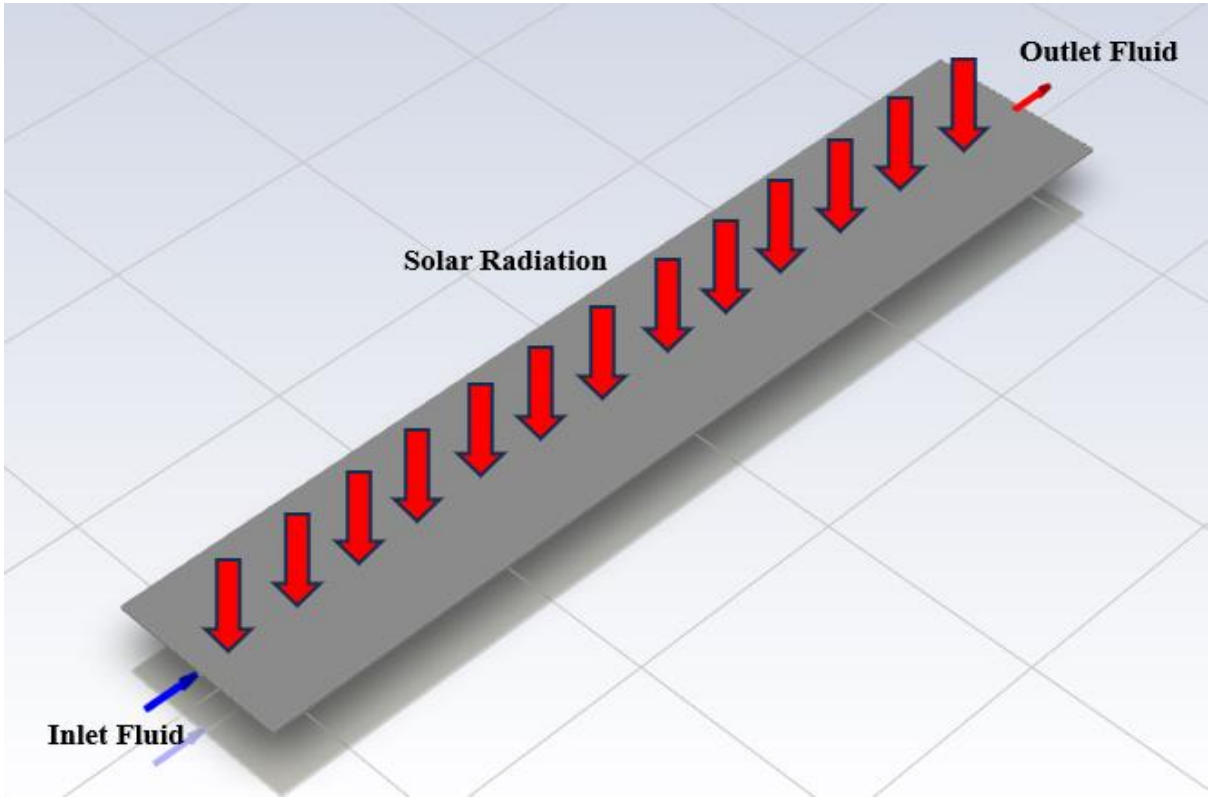

Fig. 2. Boundary conditions of the present study presented in ANSYS Fluent software

Table 3
Boundary conditions in form of mathematical equations

Tube Inlet	Tube Outlet	Solid-Fluid Interface
$\mathbf{u_x = u_{in}}$ $\mathbf{u_y = u_z = 0}$ $\mathbf{T = T_{in}}$	$P = P_{atm}(\text{static pressure})$	$u_x = u_y = u_z = 0$ $q = \frac{-kdT}{dz} = h(T - T_{bulk})$

Table 4
The parameter of PVT component

Components	Parameters	Reference
Glass Case	Density, $\rho = 2200\ \mathrm{kg/m^3}$ Thermal conductivity, $k = 1.3\ \mathrm{W/mK}$ Specific heat capacity, $c_p = 749\ \mathrm{J/kgK}$ Glass emissivity = 0.88	Filipović *et al.,*[19]
Photovoltaic panel	Density, $\rho = 2330\ \mathrm{kg/m^3}$ Thermal conductivity, $k = 148\ \mathrm{W/mK}$ Specific heat capacity, $c_p = 700\ \mathrm{J/kgK}$ Absorptance of PV plate = 0.9 Emissivity of PV plate = 0.88 Temperature coefficient, $\beta_r = 0.0045^{o}\mathrm{C}^{-1}$ PV module efficiency, $\eta_r = 12\%$ at$0\ ^{o}\mathrm{C}$	Khanjari *et al.,* [12]
Absorber plate and tube	Material: Copper (Cu) Density, $\rho = 8978\ \mathrm{kg/m^3}$ Thermal conductivity, $k = 387.6\ \mathrm{W/mK}$ Specific heat capacity, $c_p = 381\ \mathrm{J/kgK}$	

2.3 Simulation Assumptions

Table 5 summarizes the simulation assumptions underlying the present study.

Table 5
Simulation assumption for present study

No	Assumptions
1	The fluid flow under study is characterized as steady-state, incompressible, and uniform
2	The nanofluid flow regime is characterized as laminar at the inlet and fully developed at the outlet in terms of both thermal and dynamic aspects.
3	The thermal equilibrium between base fluid and nanoparticles has been taken into consideration, resulting in the incorporation of a single-phase nanofluid in the computation results. However, nanoparticles and base fluids exist as two distinct phases in their actual condition; hence, nanofluids should exhibit the characteristics of base fluids.
4	The internal layer's temperature between the PV panel and absorber plate is estimated to be identical, as the ideal interface is assumed for both components.
5	It is predicted that a certain amount of solar energy is absorbed by PV cells and converted into electrical energy, while the remaining energy leads to the PV cells temperature increment.
6	The incident solar radiation is assumed to be perpendicular and consistent with the uppermost PV model, which is the glass case
7	The radiation heat loss in the absorber plate and tube is neglected due to the extremely low temperatures
8	Both the absorber plate's bottom surface and the tube's external surface are assumed to be adiabatic.
9	The contact resistance between the glass case, PV panel, absorber plate, and collector is neglected.
10	The thickness of the adhesive layer between the photovoltaic panel and the absorber plate is neglected.

2.4 Governing Equations

The governing equations play a crucial role in this study as they provide the theoretical framework for the CFD simulation. The numerical research on nanofluids typically involves the resolution of the conservation laws, which can be categorised into three fundamental laws: energy conservation, momentum conservation, and continuity conservation. In general, the CFD methodology for addressing conservation laws entails three main stages. The initial stage involves organising the

conservation equations within the computational domain. The subsequent stage involves the conversion of differential equations into algebraic equations through the implementation of discretization techniques. The final stage entails the utilisation of iterative approaches to resolve the algebraic equations. After that, the prevailing problem's domain is discretized into a finite collection of control volumes, and the governing equations are resolved through the finite volume method [20]. The three-dimensional steady-state governing equations of mass (continuity), momentum (Navier-Stokes), and energy are presented in Table 6.

Table 6
The three-dimensional steady-state governing equations

Conservation Laws	Conservation Equations	
Continuity	$\nabla(\rho_{nf}U_{nf}) = 0$	(2)
Momentum	$\nabla \cdot (\rho_{nf}U_{nf}U_{nf}) = -\nabla P + \nabla\tau + \rho_{nf}g$	(3)
Energy	$\nabla \cdot \left(\rho_{nf}U_{nf}C_{p_{nf}}T\right) = \nabla(k_{nf}\nabla T)$	(4)

For the Eq. (2), Eq. (3) and Eq. (4), $P, \tau, \rho_{nf}, U_{nf}, C_{p_{nf}}, k_{nf}, T, g$ represent the pressure, transmittivity, nanofluid density, nanofluid velocity, nanofluid specific heat capacity, nanofluid conductivity, temperature, and gravity acceleration, respectively [21].

2.5 Numerical Method and Solver Setting

This research study implements the ANSYS FLUENT software for simulation and verification purposes. The bulk of solar irradiation utilized as input energy is assimilated by the photovoltaic module, with a fraction of it being dissipated through conduction, convection and radiation coming from the photovoltaic surface. Then, the heat energy that has been assimilated is transmitted to the operational fluid to generate thermal energy. Based on the experimental studies Khanjari *et al.,* [12] the fluid flow is classified as laminar since the Reynolds number is below 2300. The pressure-based approach is utilized in the laminar PVT model. The steady-state solver is employed to compute numerical equations. Even though transient solvers involve solving time-dependent equations to model dynamic behaviour over time, the simulations conducted in the present study were executed under steady-state conditions to reduce computational costs and time. Meanwhile, research has indicated that the disparity in result precision between steady and transient simulations is relatively low, with a just 0.2% variance [22]. The SIMPLE scheme (Semi-Implicit Method for Pressure-Linked Equations) is implemented to provide the pressure-velocity coupling. The second order upwind method is selected as the interpolation scheme to discretize the convection and diffusion variables. The measurement of solution variable gradients at the cell centre is accomplished through a least squares cell-based approach. The iteration solutions are assumed to be converged when the residual values are lower than 10^{-4} for continuity, 10^{-3} for momentum and 10^{-6} for energy equations. The atmospheric temperature variations, and wind velocity are neglected during the simulation.

2.6 Working Fluid Properties
2.6.1 Thermophysical properties of base fluid

The present study utilized pure water as the base fluid, while incorporating silver, zinc oxide and silicon oxide nanoparticles as the nanomaterials. Table 7 shows the temperature-dependent correlations of base fluid at various operational temperatures for the determination of their thermophysical characteristics.

Table 7
The correlations for thermophysical properties of base fluid

Properties	Correlation		References
Density $\boldsymbol{\rho_{bf}}$	$\rho_{bf} = -4.48 \times 10^{-3}T^2 + 999.9$	(5)	Hosseinzadeh *et al.,* [14]
Viscosity $\boldsymbol{\mu_{bf}}$	$\mu_{bf} = \exp\left[-1.6 - \frac{1150}{T} + (\frac{690}{T})^2\right] \times 10^{-3}$	(6)	
Thermal Conductivity $\mathbf{k_{bf}}$	$k_{bf} - 8.01 \times 10^{-6}T^2 + 1.94 \times 10^{-3}T + 0.563$	(7)	
Specific Heat Capacity $\mathbf{C_{p,bf}}$	$C_{\rho,bf} = -0.0000463T^3 + 0.0552T^2 - 20.86T + 6719.637$	(8)	Kell *et al.,* [23]

For the Eq. (5), Eq. (6), Eq. (7) and Eq. (8), $\rho_{bf}, \mu_{bf}, k_{bf}, C_{p,bf}$ and T represent the base fluid density, base fluid viscosity, base fluid thermal conductivity, base fluid specific heat and operational fluid temperature respectively.

2.6.2 Thermophysical properties of nanofluid

Table 8 displays the overview of mathematical correlation utilized in the determination of the thermophysical properties of nanofluids. This research study evaluates the correlations between nanoparticle size, nanoparticle weight fraction, temperature dependency, and base fluid features. The present study employs two dynamic thermal conductivity approaches: the first approach for metal nanoparticles (Ag) and the second approach for metal oxide nanoparticles $(ZnO \ \& SiO_2)$. On the other hand, the effective thermal conductivity of zinc oxide and silicon oxide nanoparticles are determined by an altered equation that involves both static and Brownian motion. The nanoparticles ZnO and SiO_2 were chosen for the present study due to the comprehensive information provided, including the nanoparticle size diameter and the correlation of the temperature coefficient, β [24].

Table 8
Values of β for different nanoparticles

Type of nanoparticle	$\boldsymbol{\beta}$	Concentration (%)	Temperature (K)
$\mathbf{SiO_2}$	$1.9526(100\varphi)^{-1.4594}$	$1\% \leq \varphi \leq 10\%$	$298K \leq T \leq 363K$
ZnO	$8.4407(100\varphi)^{-1.07304}$	$1\% \leq \varphi \leq 10\%$	$298K \leq T \leq 363K$

Table 9 presents the correlations for the thermophysical properties exhibited by nanofluid. In general, an increase in the volume concentration of nanoparticles leads to an increase in the density, viscosity, and thermal conductivity of nanofluids. Einstein's equation is used to define the viscosity of nanofluids with volumetric concentrations below 5%, whereas the Batchelor model, a modified version of Einstein's equation, is employed for concentrations exceeding 5%. The process of Brownian motion is characterized by the random displacement exhibited by suspended nanoparticles in a fluid medium, and it is an essential element of the viscosity framework proposed by Batchelor [25].

Table 9
The correlations for thermophysical properties of nanofluid

Properties	Correlation		References
Density, ρ_{nf}	$\rho_{nf} = (1-\varphi)\rho_{bf} + \varphi\rho_{np}$	(9)	Mohd Rosli *et al.,* [26]
Viscosity,μ_{nf}	For $\varphi < 0.05$, $\mu_{nf} = (1+2.5\varphi)\mu_{bf}$	(10)	Mishra *et al.,* [27]
	For $0.05 < \varphi < 0.1$, $\mu_{nf} = (1+2.5\varphi+6.5\varphi^2)$	(11)	
Thermal Conductivity,k_{nf}	Method 1 $k_{nf1} = k_{bf}\frac{k_{np}+2k_{bf}-2(k_{bf}-k_{np})\varphi}{k_{np}+2k_{bf}+(k_{bf}-k_{np})\varphi} + \frac{\rho_{np}\varphi C_{p,bf}}{2k_{bf}}\left(\sqrt{\frac{2k_B T}{3\pi d_{np}\mu_{bf}}}\right)$	(12)	Xuan *et al.,* [28]
	Method 2 $k_{nf2} = k_{static} + k_{brownian}$ $k_{static} = k_{bf}\frac{k_{np}+2k_{bf}-2(k_{bf}-k_{np})\varphi}{k_{np}+2k_{bf}+(k_{bf}-k_{np})\varphi}$ $k_{brownian} = A_1\sqrt{T}(A_2 T + A_3)$ $A_1 = 5*10^4\beta\varphi\rho_{bf}C_{p,bf}\sqrt{\frac{k_B}{d_{np}\rho_{np}}}$ $A_2 = \frac{2.8217*10^{-2}\varphi + 3.917*10^{-3}}{273}$ $A_3 = -3.0669*10^{-2}\varphi - 3.9113*10^{-3}$ $\beta_{ZnO} = 8.4407(100\varphi)^{-1.07304}$ $\beta_{SiO^2} = 1.9526(100\varphi)^{-1.4594}$ $k_{nf2} = k_{bf}\frac{k_{np}+2k_{bf}-2(k_{bf}-k_{np})\varphi}{k_{np}+2k_{bf}+(k_{bf}-k_{np})\varphi} + 5*10^4\beta\varphi\rho_{bf}C_{p,bf}\sqrt{\frac{k_B T}{d_{np}\rho_{np}}\cdot f(T,\varphi)}$	(13)	Seyf & Nikaaein [29] & Hasan *et al.,* [19]
Specific Heat Capacity, $C_{\rho,nf}$	$C_{p,nf} = \frac{(1-\varphi)\rho_{bf}C_{p,bf} + \varphi\rho_{np}C_{p,np}}{\rho_{nf}}$	(14)	Kakaç & Pramuanjaroenkij [30]

For Eq. (9), $\rho_{nf}, \rho_{bf}, \rho_{np}, \text{and } \varphi$ represent the nanofluid density, base fluid density, nanoparticle density and nanoparticle volume fraction. For Eq. (10) and Eq. (11), $\mu_{nf}, \mu_{bf} \text{ and } \varphi$ represent the nanofluid viscosity, base fluid viscosity and nanofluid volume fraction respectively. For Eq. (12) and Eq. (13), $k_{nf1}, k_{nf2}\ k_{bf}, k_{np}, \rho_{np}, \varphi, C_{p,bf}, T, d_{np} \text{ and } \mu_{bf}$ represent the nanofluid thermal conductivity for method 1, nanofluid thermal conductivity for method 2, base fluid thermal conductivity, nanoparticle thermal conductivity, nanofluid volume fraction, base fluid specific heat, nanofluid temperature, nanoparticle diameter and base fluid viscosity. k_B is Boltzmann constant $(1.3807 \times 10^{-23} \frac{j}{K})$.The parameter f considers the rise in temperatures resulting from particle interactions. On the other hand, function β denotes the proportion of the nanofluid and exhibits a decreasing trend as the particle volumetric concentration increases, due to the viscous effect of particles in motion.

For Eq. (14), $C_{p,nf}, C_{p,bf}, C_{p,np}, \rho_{nf}, \rho_{bf}, \text{ and } \varphi$ represent the nanofluid specific heat capacity, base fluid specific heat capacity, nanoparticle specific heat capacity, nanofluid density, nanoparticle density, base fluid density and nanofluid volume fraction, respectively. Table 10 shows the thermophysical properties of both nanoparticles and base fluid, whereas Table 11 displays the thermophysical properties of the nanofluid employed in the current investigation.

Table 10
The thermophysical properties of nanoparticles and base fluid

Properties	Pure Water ($\mathbf{H_2O}$)	Zinc Oxide (ZnO)	Silicon Oxide ($\mathbf{SiO_2}$)
Density, $\boldsymbol{\rho}$ $(\frac{\mathbf{kg}}{\mathbf{m^3}})$	992.8	5600	2200
Thermal Conductivity, k $(\frac{\mathbf{W}}{\mathbf{mK}})$	0.6275	13	1.2
Specific Heat, $\mathbf{c_p}$ $(\frac{\mathbf{J}}{\mathbf{kgK}})$	4179	495.2	703

Table 11
The thermophysical values of nanofluid

Volume fraction, $\boldsymbol{\varphi}$ (%)	$\mathbf{ZnO - water\ nanofluid}$				$\mathbf{SiO_2 - water\ nanofluid}$			
	ρ_{nf}	$C_{\rho f}$	k_{nf}	μ_{nf}	ρ_{nf}	$C_{\rho f}$	k_{nf}	μ_{nf}
0	992.8	4179	0.6275	0.00066	992.8	4179	0.6275	0.00066
1	1038.87	3980.43	0.685	0.00068	1004.87	4102.91	0.647	0.00068
2	1084.94	3798.73	0.701	0.00069	1016.94	4028.62	0.6476	0.00069
3	1131.02	3631.8	0.7178	0.00071	1029.02	3956.04	0.6505	0.00071
4	1177.09	3477.97	0.7354	0.00073	1041.09	3885.18	0.6539	0.00073
5	1223.16	3335.72	0.7536	0.00074	1053.16	3815.94	0.6578	0.00074
6	1269.23	3203.8	0.7721	0.00078	1065.23	3748.27	0.662	0.00078
8	1361.38	2966.73	0.8103	0.00082	1089.38	3617.4	0.6703	0.00082
10	1453.52	2759.74	0.8498	0.00087	1113.52	3492.24	0.679	0.00087

2.7 Thermodynamic Analysis

In general, thermodynamic analysis is a systematic approach that encompasses the analysis of energy. The field of energy analysis is concerned with the measurement of energy transfers within a system. Energy analysis corresponds to the study of energy transfer and conversion within a system and is established based on the first law of thermodynamics. According to the first law of thermodynamics, energy is conserved and cannot be generated

or annihilated; it can only be transformed or transferred from one state to another. Hence, the PV/T system's electrical and overall efficiencies can be determined by utilising the conservation balance equations, and the calculation is performed as follows:

$$\eta_{thermal} = \frac{\dot{m}_{nf} C_{p,nf} (T_{out} - T_{in})}{G_t A_{ct} \tau_g \alpha_{cell}} \quad (15)$$

$$\eta_{electrical} = \eta_{ref}[1 - \beta(T_{cell} - T_{ref})] \quad (16)$$

$$\eta_{overall} = \eta_{thermal} + \eta_{electrical} \quad (17)$$

For the Eq. (15), Eq. (16) and Eq. (17) , $\eta_{overall}, \eta_{thermal}, \eta_{electrical}, \dot{m}_{nf}, C_{p,nf}, T_{out}, T_{in}, G_{t,}$ $A_{ct}, \tau_g,$ $\alpha_{cell}, \eta_{ref}$ and β represent the overall efficiency, thermal efficiency, electrical efficiency, nanofluid mass flow rate, nanofluid specific heat capacity, outlet temperature, inlet temperature, solar radiation intensity, area of collector tube, glass cover transmissivity, PV cells absorptivity, PV module electrical efficiency at standard test condition and temperature coefficient respectively. The subscript “nf” refers to the nanofluid used in the present study.

2.8 Meshing

After completion of the PVT model construction in SolidWorks, a three-dimensional meshing process is executed to facilitate the resolution of the governing partial differential equations within the allocated cell. A tetrahedron mesh was generated for the optimized grid using the patch-conforming mesh method within the fluid body domain. The sweep method is applied to the PV module to refine the mesh, ensure solver accuracy, and accelerate the solving process. At the same time, inflation features are employed on the fluid domain region surrounding the absorber tube to enhance the solver's accuracy close to the working fluid regions. In addition, body sizing is applied to the glass case, PV panel and absorber plate to enhance the mesh quality of the PVT models. The PVT model meshing incorporates capture curvature and capture proximity techniques to effectively capture flow features near boundaries or interfaces. This approach ensures a precise simulation outcome by accurately capturing the behaviour of the boundary layer. Figure 3 show the front view of the PVT model meshing result.

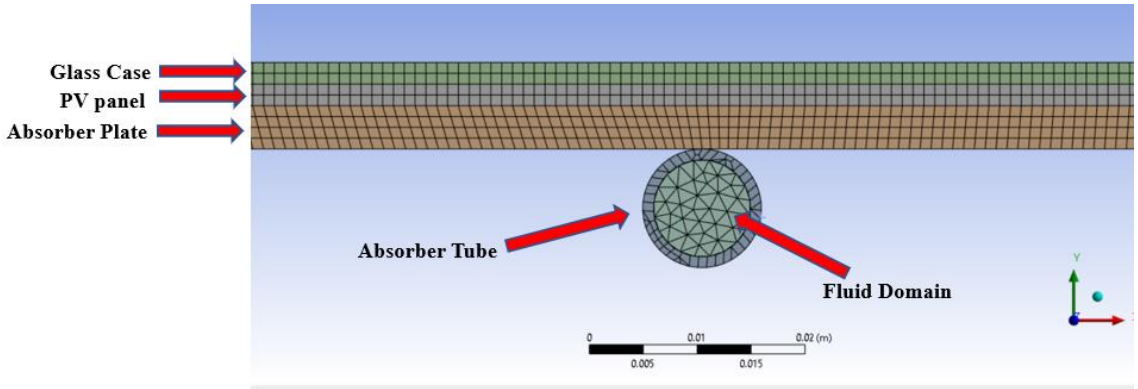

Fig. 3. Front view PVT model meshing

After that, a mesh evaluation is performed on the produced mesh to ascertain whether the PVT mesh model is capable of resulting in reliable results in ANSYS CFD Fluent. The PVT

mesh model generated through the ANSYS Meshing comprises 781898 nodes and 847371 elements. The reported PVT meshed model exhibits an average skewness of 0.1185 and an average orthogonal quality of 0.91701. Therefore, it can be concluded that the mesh quality of the model is reliable and satisfactory for simulation in ANSYS Fluent software.

2.9 Grid Independence Test

The objective of this grid independence test is to determine the optimum element size for obtaining accurate and reliable results without reducing their precision. Table 12 displays the mesh distribution of the PVT model with varying element sizes. Figure 4 illustrates the grid independence test graph of outlet temperature against the number of elements of the PVT modal. It reveals that the outlet temperature increases significantly with increasing mesh count during the initial phase but only increases slightly at the final stage. This indicates that as the number of cells increases, the mesh becomes finer; however, the increase in precision becomes insignificant once the limit is reached.

The calculation of the relative error associated with the finer mesh can be accomplished by utilizing Eq. (18), where e_{fine} refer to the relative error, $\phi_1 and\, \phi_2$ denote the flow quantities associated with diverse parameters, such as velocity, temperature, and pressure, for the finer and coarser mesh, respectively. In this simulation study, the outlet temperature represents the selected flow quantities and relative errors below 5% are generally considered acceptable. Therefore, mesh case 4 with 847371 of cell was selected for the CFD simulations employed in this study to minimize computational cost and simulation duration while preserving the result's precision.

$$e_{fine} = \left|\frac{\phi_1 - \phi_2}{\phi_1}\right| \tag{18}$$

Table 12
Grid independence test for different mesh sizes

Mesh Cases	No of element	Outlet temperature (K)	Relative Error (%)
1	325281	328.038	-
2	417165	328.048	0.00305
3	474477	328.052	0.00152
4	847371	328.079	0.00792
5	1368435	328.082	0.00091

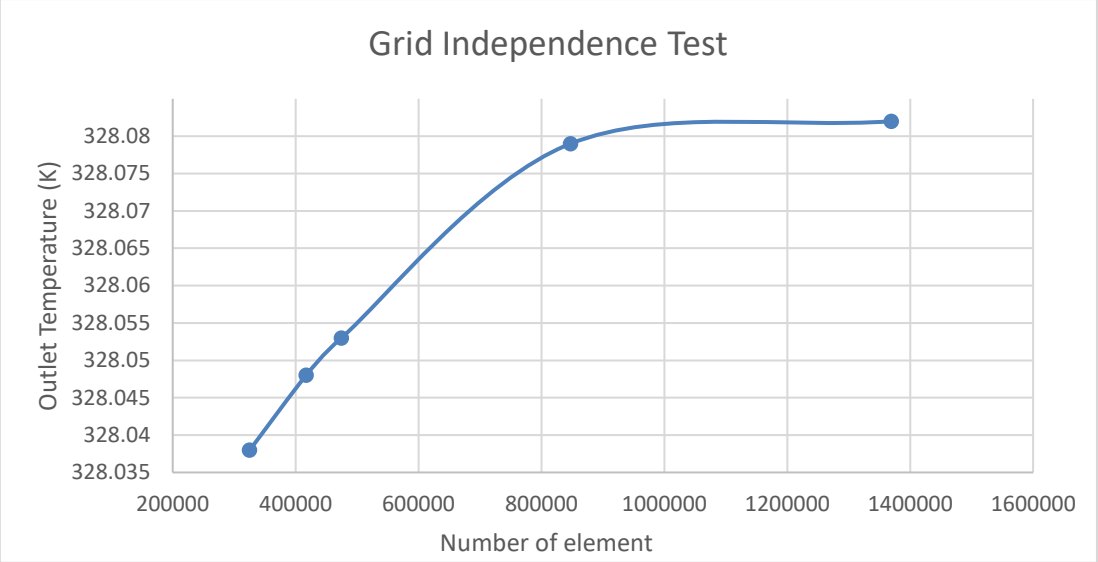

Fig. 4. Grid independence test

3. Results

3.1 Result Verification

The present study's simulation results have been verified through the existing numerical study of the PVT system. The verification of this model is conducted under the base case conditions specified by Khanjari *et al.,* [12] in their research. In instances where the parameter is not specified, a comparative analysis was conducted among the existing research literature and personal assumptions to establish the CFD simulation framework. The boundary conditions for the verification simulation setup are summarised below in Table 13.

Table 13
Boundary conditions for verification simulation setup

Parameters	Initial boundary conditions
Nanofluid inlet velocity	0.06377 m/s
Nanofluid inlet temperature	$30^{o}C$
Total solar radiation	$800W/m^2$
Nanofluid volumetric concentration	5%
Density of Ag-water nanofluid, $\boldsymbol{\rho_{nf}}$	$1467.6\,\frac{kg}{m^3}$
Specific heat capacity of Ag-water nanofluid, $\boldsymbol{C_{p,nf}}$	$2768.2\,\frac{J}{kgK}$
Thermal conductivity of Ag-water nanofluid, $\boldsymbol{k_{nf}}$	$1.2461\,\frac{W}{mK}$
Dynamic viscosity of Ag-water nanofluid, $\boldsymbol{\mu_{nf}}$	$0.000741\,\frac{kg}{ms}$

3.1.1 Qualitative result verification

The Ag-water nanofluid temperature distribution at the absorber tube's outlet region is compared in Figure 5(a) and Figure 5(b) between the existing study and the present study. The temperature distribution observed in the present study possesses a similar temperature contour to that reported in the verified literature, thereby confirming the precision of the research outcomes**.** It appears that the temperature rises along the paths from the tube's

centre to its wall and from the inlet to its outlet for both temperature contour. This is because heat is transmitted from the PV panel to the absorber tube where the outer surface of the absorber tube is attached to the absorber plate, as the thickness of the adhesive material between the PV panel and the absorber plate is ignored during the CFD simulation. Therefore, the temperature contour of the absorber tube reveals an excess temperature along the tube's edge, especially in the contact region between the absorber tube and the absorber plate.

In comparison to the symmetrical outlet temperature distribution of the existing study in Figure 5(a), the present study in Figure 5(b) reveals an asymmetrical outlet temperature distribution that leads to the formation of noticeable hotspot regions. Varying meshing methods employed on the circular tube, in comparison with preference research, might have contributed to the observed asymmetrical outlet temperature contour in this study. The meshing technique implemented was derived from other research papers, as the reference paper does not provide specific information regarding the meshing procedure. Circular meshing may alter the discretization of the solution domain, thus affecting the patterns of heat transfer and fluid flow along the absorber tube. Meanwhile, variances in mesh density and resolution may impact the simulation's precision, as insufficient mesh refinement could potentially fail to capture specific details, whereas excessive refinement might result in escalated computational times [31].

Conversely, it is observed that the outlet temperature of the present study exhibits a greater temperature compared to the reference paper when the maximum and minimum temperature are established at 328.3K and 318.4K, respectively. The average outlet temperature for the computed geometry and reference model, based on the simulation setup under the initial boundary conditions, is 326.082K and 320.865K, respectively. The percentage difference of the outlet temperature between the results obtained from the present study and the numerical simulation is 1.63%. The observed disparity in temperature range between the current investigation and the verified study could potentially be attributed to unspecified parameters, such as the specific dimensions of each PVT component and the thermophysical properties of the PVT material. Despite that, both the temperature contours exhibit a compatible flow pattern, thereby verifying the PVT model mechanism.

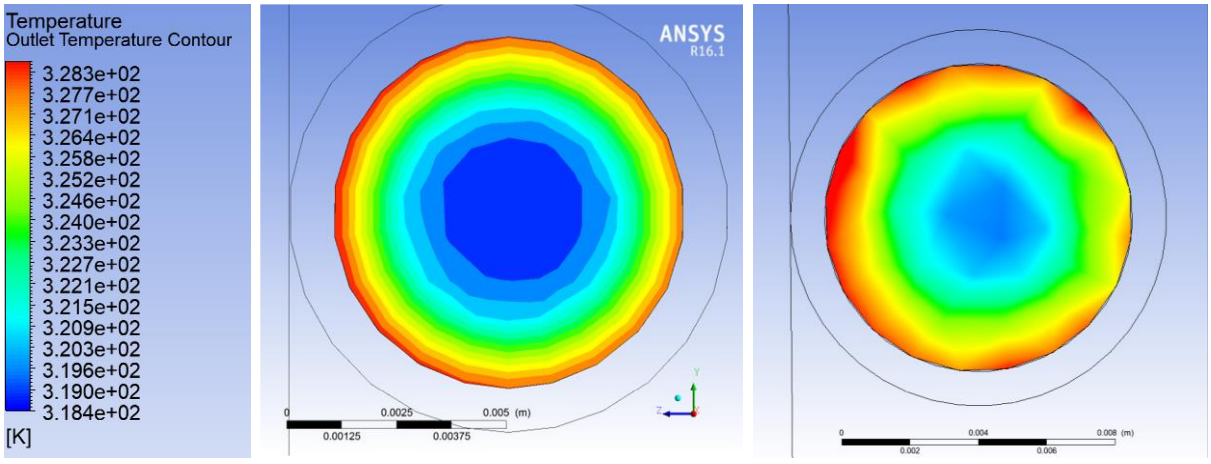

(a) (b)

Fig. 5. Outlet temperature distribution of the (a) existing study and (b) present study

3.1.2 Quantitative result verification

The coolant fluid utilised in this PVT system is a volumetric concentration of 5% Ag-water nanofluid, which is incorporated at inlet velocities comprising from 0.05 m/s to 0.23 m/s. The results of outlet temperature against inlet velocity are compared and presented in Figure 6. The present study demonstrates a greater outlet temperature in relation to the numerical results for every inlet velocity parameter. The maximum and minimum percentage error from both the present study and the numerical result are recorded, where the maximum and average deviations are 1.44% and 1.06%, respectively. Furthermore, the mean average percentage error (MAPE) is computed to assess the precision of the simulation outcomes relative to the experimental data. The MAPE is computed by dividing the sum of all errors by the total number of study observations. The MAPE for the outlet temperature of Ag-water nanofluid is 1.21%. Therefore, the agreement between the cited research and the present study is strong, as the percentage difference is below 5%. Therefore, the reliability of PVT modals is verified, and further simulation analyses are permissible for the current study.

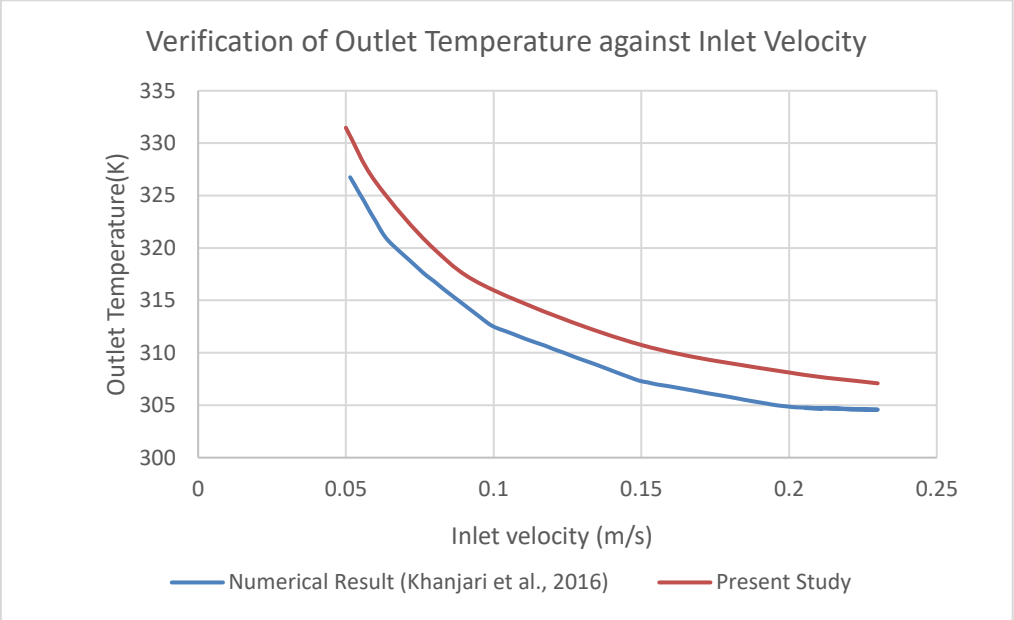

Fig. 6. Verification of outlet temperature against inlet velocity between present study and numerical results

3.2 Simulation Study

3.2.1 Nanofluid volumetric concentration

In the present study, ZnO and SiO_2 nanoparticles are dispersed in the base fluid of water. The nanoparticles vary in volumetric concentration, ranging from 1% to 10%, while conserving a constant solar radiation of $800 \mathrm{Wm}^{-2}$, an inlet fluid velocity of 0.1 m/s, a nanoparticle diameter of 50 nm, and an inlet fluid temperature of 303.15 K. In general, dispersing nanoparticles in the base fluid enhances the effective thermal conductivity of the nanofluid through Brownian motions, particle-particle collisions, and liquid stratification mechanisms**.** The nanofluid creates thermal turbulence, enhancing the thermal transfer rate. Additionally, dispersing nanoparticles into the base fluid leads to an increase in thermal conductivity and a thickening of the boundary layer near the tube surfaces, which results in a significant

temperature gradient. Figure 8(a) displays the outlet temperature of the PVT system incorporating ZnO-water nanofluid and SiO_2-water nanofluid for various volumetric concentrations. As the volumetric concentration increases, both nanofluids' temperature exhibit a rising trend. According to the reported data, the outlet temperatures for ZnO-water and SiO_2-water nanofluid are 319.14K and 319.019K at 1% volume fraction and 319.527K and 319.219K at 10% volume fraction. Therefore, the ZnO nanoparticle exhibits a more substantial increase in outlet temperature and gradient increment compared to the SiO_2 nanoparticle. Figure 7(a) illustrates the temperature distribution at the outflow of the ZnO-water nanofluid with varying volumetric concentrations. It reveals that as the volumetric concentration of the ZnO-water nanofluids increased, the outlet temperature correspondingly increased, especially in the fluid flow centre region. This is because the thermal conductivity and density of the ZnO-water nanofluid increase with the volumetric concentration increment, thereby enhancing its heat transmission capability.

As the volume fraction increased from 1% to 10%, both nanofluids exhibited a reduction in photovoltaic temperature, as shown in Figure 8(b). The ZnO-water nanofluids exhibit a noticeable reduction along a steeper decline curve of PV temperature compared to the SiO_2-water nanofluid. The data presented indicates that the total PV temperature reductions for ZnO-water and SiO_2-water nanofluid are 0.994K and 0.358K, respectively, ranging from 1% to 10%. The result indicates that ZnO-water nanofluid outperforms SiO_2-water nanofluid in terms of facilitating heat dissipation within the PV panel. The PV cell temperature distribution of the ZnO-water nanofluid across various volumetric concentrations is illustrated in Figure 7(b). The data indicates that an increase in volumetric concentration of ZnO-water nanofluids results in a corresponding decrease in PV cell temperature. This is because an increase in volumetric concentration results in a reduction in specific heat capacity and an accompanying rise in density, thermal conductivity, and dynamic viscosity. As a result, the coefficient of convection, h is increased for the nanofluids with greater volume fractions for heat transfer along the PVT system. The enhanced thermal conductivity and density of the nanofluid facilitate a more efficient transmission of heat energy from the heated surface, resulting in a higher heat transfer rate. This is because the nanofluid's higher thermal conductivity minimises the temperature gradient within the boundary layer of the fluid, thus facilitating effective heat transfer. In general, nanofluids with greater specific heat possess the ability to absorb more energy before encountering significant variations in temperature. When the volumetric concentration of the nanofluid increases and the specific heat capacity decreases, the PVT system encounters an increase in heat transfer and a greater coefficient of convection.

As illustrated in Figure 9(a), the thermal efficiency demonstrates an upward trend as the volumetric concentration of the nanofluid increases. The ZnO-water nanofluid reveals enhanced thermal efficiency compared to the SiO_2-water nanofluid due to its superior thermal conductivity and enhanced heat transfer capabilities along the absorber tube. The enhanced thermal conductivity of nanofluids leads to a reduction in boundary layer resistance and facilitates better heat transfer from the collector to the fluid, further improving thermal efficiency. However, the presented improvement to thermal efficiency is insignificant, as the total enhancement for ZnO-water and SiO_2-water nanofluid is merely 0.39% and 0.216%, respectively, ranging from 1% to 10%.

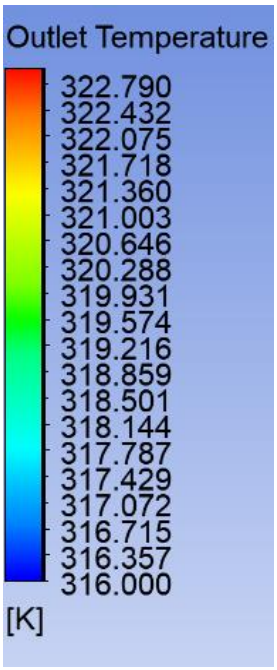

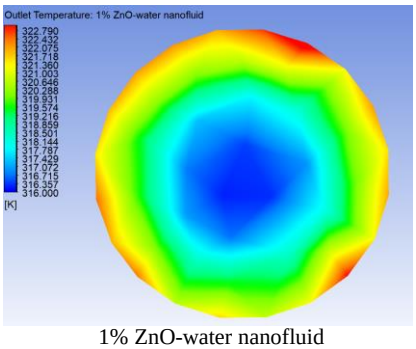

1% ZnO-water nanofluid

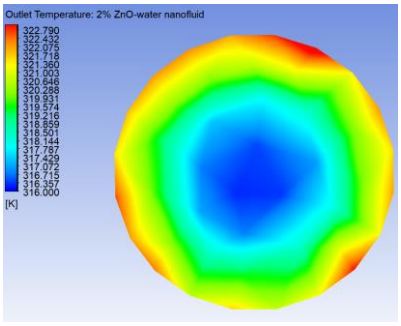

2% ZnO-water nanofluid

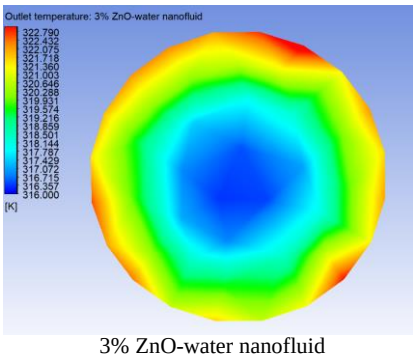

3% ZnO-water nanofluid

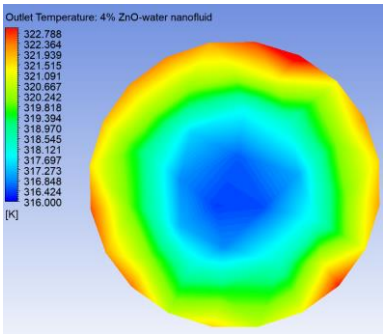

4% ZnO-water nanofluid

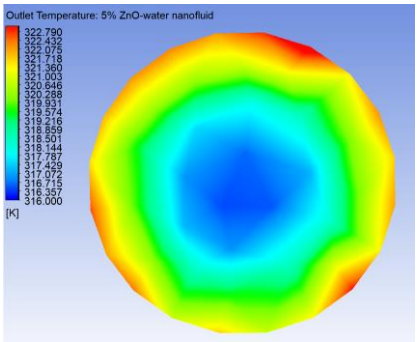

5% ZnO-water nanofluid

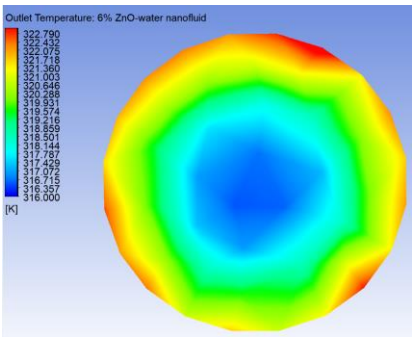

6% ZnO-water nanofluid

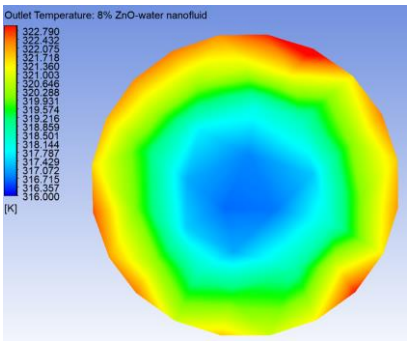

8% ZnO-water nanofluid

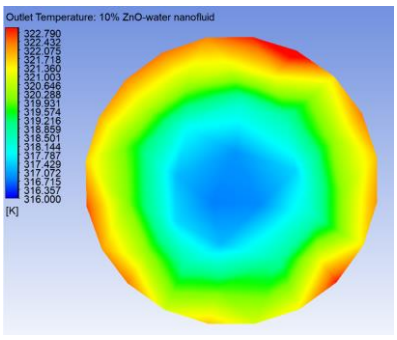

10% ZnO-water nanofluid

(a)

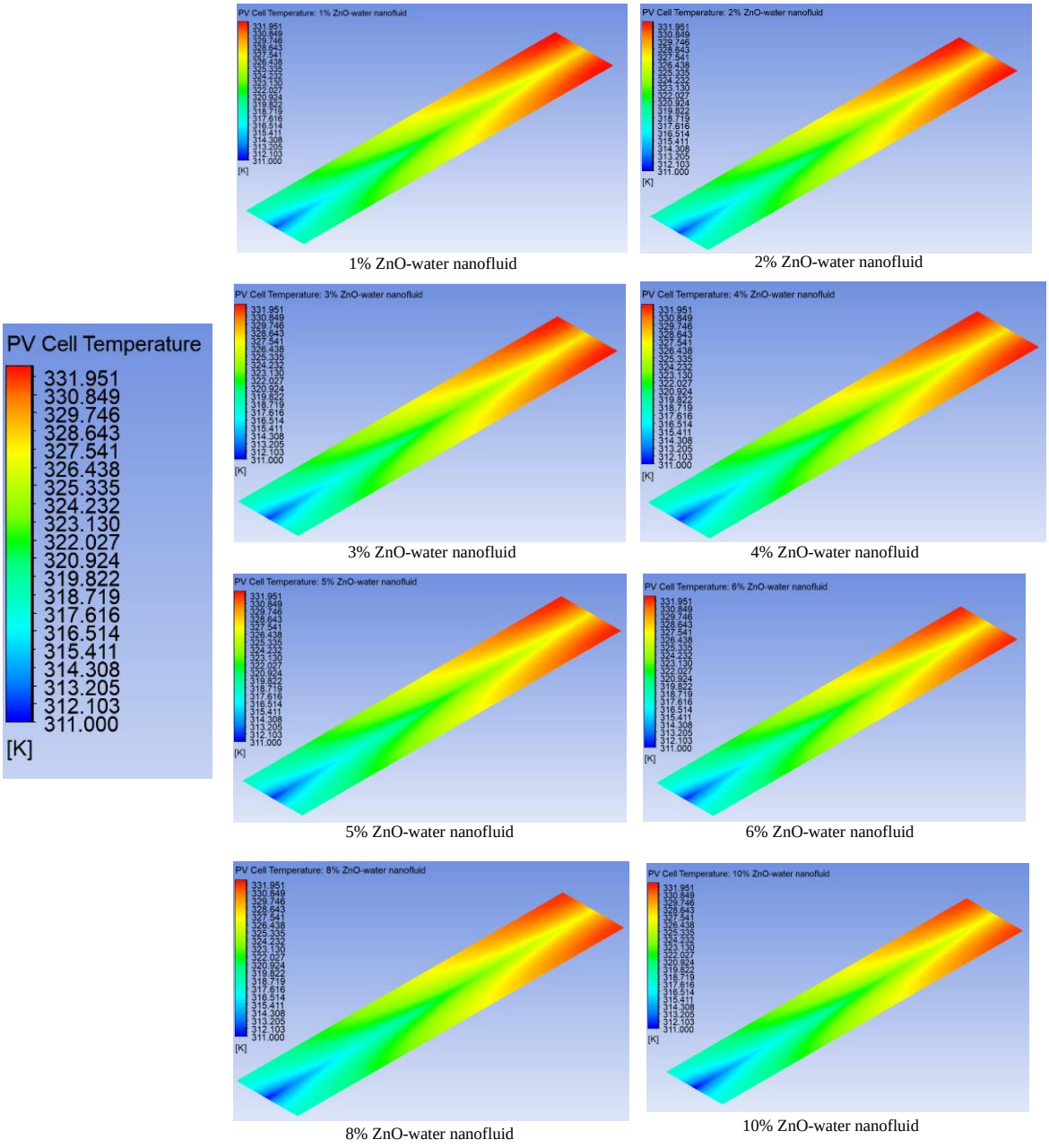

(b)

Fig. 7. Outlet temperature (a) and PV cell temperature (b) distribution of ZnO-water nanofluids against varies volumetric concentration

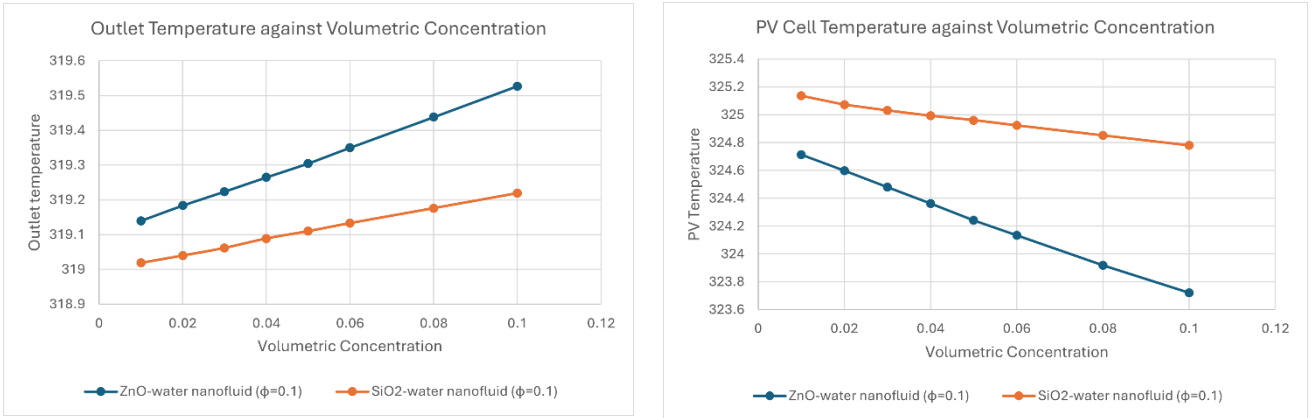

(a) (b)

Fig. 8. Graph of outlet temperature (a) and PV cell temperature (b) against nanofluid's volumetric concentration

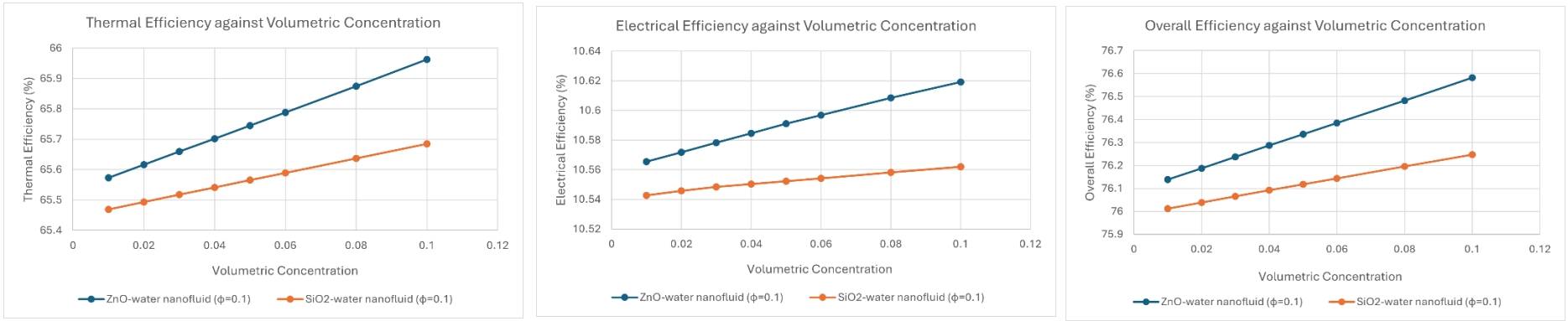

(c) (d) (e)

Fig. 9. Graph of thermal efficiency (a), electrical efficiency (b) and overall efficiency against nanofluid's volumetric concentration

As illustrated in Figure 9(b) the electrical energy efficiency of the PVT system rises as the volume fraction of the nanoparticle increases. The ZnO-water nanofluid demonstrates a greater degree of upward trend in its electrical efficiency as compared to the SiO_2-water nanofluid. This is because the ZnO-water nanofluid has a greater heat transfer coefficient, which reduces the PV cell temperature and facilitates the cooling process of the PV panel, thereby enhancing power generation. As depicted in Figure 9(c), the overall efficiency of the PVT system increases steadily with the nanoparticle volume fraction. The data presented indicates that the overall efficiency of ZnO-water nanofluid and SiO_2-water nanofluid is 76.14% and 76.01% at 1% volume fraction, and 76.58 and 76.25% at 10% volume fraction. However, PVT performance in real conditions will be reduced if the volumetric concentration of nanofluid is exceeded due to the precipitation and coagulation of nanoparticles. The excess nanoparticles will aggregate due to the attractive force between the nanoparticles and sedimentation if the nanofluid remains undisturbed for a longer period. Precipitation-induced particle agglomeration reduces the thermal conductivity of the nanofluid and fluid flow, thereby lowering the heat transfer efficiency within the PVT system.

4. Conclusion

The present study presents a numerical investigation of a photovoltaic thermal system with nanofluid via CFD FLUENT software. The validity of the results obtained in the present has been verified; the deviation is less than 5%. Outcomes show that increasing the volumetric concentration of nanofluids improves the PVT efficiency and it is demonstrated that ZnO-water nanofluid outperforms SiO_2-water nanofluid. Conversely, the ZnO-water nanofluid exhibits greater effectiveness in all phases in comparison to the SiO_2-water nanofluid at volumetric concentrations ranging from 1% to 10%. The ZnO-water nanofluid demonstrates greater thermal conductivity and density, in comparison to the SiO_2-water nanofluid, which leads to an increase in the coefficient of convection. However, insignificant efficiency improvement is observed for both ZnO-water nanofluid and SiO_2-water nanofluid with 0.444% and 0.235% growth, respectively, when the volumetric concentration increases to 10%. However, it is important to acknowledge certain limitations of the current study, as they merely involve a simulation study without incorporating any experimental analysis. Future research should focus on evaluating actual experiments in order to evaluate the performance of nanofluid-based PVT in actual conditions with a more reliable result. Hence, future research should incorporate both experimental work and simulation studies into the PVT research. Additionally, it is crucial to enhance the stability of nanofluids and reduce the cost of nanofluid production through the development of large-scale production techniques.

Acknowledgement

The authors would like to thank Faculty of Mechanical Technology and Engineering, Universiti Teknikal Malaysia Melaka and Departemen Teknik Mesin, Institut Teknologi Sepuluh Nopember for their contributions and support to the project.

References

[1] Abdullah, Amira Lateef, Suhaimi Misha, Noreffendy Tamaldin, Mohd Afzanizam Mohd Rosli, and Fadhil Abdulameer Sachit. "A Review: Parameters affecting the PVT collector performance on the thermal, electrical, and overall efficiency of PVT system." *Journal of Advanced Research in Fluid Mechanics and Thermal Sciences* 60, no. 2 (2019): 191-232.

[2] Sachit, Fadhil Abdulameer, Mohd Afzanizam Mohd Rosli, Noreffendy Tamaldin, Suhaimi Misha, and Amira Lateef Abdullah. "Effect of a new absorber design on the performance of PV/T collector: Numerical comparative study." *Journal of Advanced Research in Fluid Mechanics and Thermal Sciences* 71, no. 1 (2020): 60-71. https://doi.org/10.37934/arfmts.71.1.6071

[3] Rosli, Mohd Afzanizam Mohd, Danial Shafiq Mohd Zaki, Fatiha Abdul Rahman, Suhaila Sepeai, Nurfaizey Abdul Hamid, and Muhammad Zaid Nawam. "F-Chart Method for Design Domestic Hot Water Heating Systemin Ayer Keroh Melaka." *Journal of Advanced Research in Fluid Mechanics and Thermal Sciences* 56, no. 1 (2019): 59-67.

[4] Yazdanifard, Farideh, Ehsan Ebrahimnia-Bajestan, and Mehran Ameri. "Investigating the performance of a water-based photovoltaic/thermal (PV/T) collector in laminar and turbulent flow regime." *Renewable Energy* 99 (2016): 295-306. https://doi.org/10.1016/j.renene.2016.07.004

[5] Choi, S. U. S., and J. A. Eastman. "Enhancing Thermal Conductivity of Fluids with Nanoparticles; United States." *Department of Energy: Washington, DC, USA* (1995).

[6] Etminan-Farooji, Vahid, Ehsan Ebrahimnia-Bajestan, Hamid Niazmand, and Somchai Wongwises. "Unconfined laminar nanofluid flow and heat transfer around a square cylinder." *International Journal of Heat and Mass Transfer* 55, no. 5-6 (2012): 1475-1485. https://doi.org/10.1016/j.ijheatmasstransfer.2011.10.030

[7] Sardarabadi, Mohammad, Mohammad Passandideh-Fard, and Saeed Zeinali Heris. "Experimental investigation of the effects of silica/water nanofluid on PV/T (photovoltaic thermal units)." *Energy* 66 (2014): 264-272. https://doi.org/10.1016/j.energy.2014.01.102

[8] Radwan, Ali, Mahmoud Ahmed, and Shinichi Ookawara. "Performance enhancement of concentrated photovoltaic systems using a microchannel heat sink with nanofluids." *Energy Conversion and Management* 119 (2016): 289-303. https://doi.org/10.1016/j.enconman.2016.04.045

[9] Said, Zid, Mohammad H. Sajid, Mohammad A. Alim, Rahman Saidur, and Nasrudin A. Rahim. "Experimental investigation of the thermophysical properties of AL2O3-nanofluid and its effect on a flat plate solar collector." *International communications in heat and mass transfer* 48 (2013): 99-107. https://doi.org/10.1016/j.icheatmasstransfer.2013.09.005

[10] Al-Waeli, Ali HA, K. Sopian, Miqdam T. Chaichan, Hussein A. Kazem, Husam Abdulrasool Hasan, and Ali Najah Al-Shamani. "An experimental investigation of SiC nanofluid as a base-fluid for a photovoltaic thermal PV/T system." *Energy Conversion and Management* 142 (2017): 547-558. https://doi.org/10.1016/j.enconman.2017.03.076

[11] Teng, Tun-Ping, Yi-Hsuan Hung, Tun-Chien Teng, Huai-En Mo, and How-Gao Hsu. "The effect of alumina/water nanofluid particle size on thermal conductivity." *Applied Thermal Engineering* 30, no. 14-15 (2010): 2213-2218. https://doi.org/10.1016/j.applthermaleng.2010.05.036

[12] Khanjari, Y., F. Pourfayaz, and A. B. Kasaeian. "Numerical investigation on using of nanofluid in a water-cooled photovoltaic thermal system." *Energy Conversion and Management* 122 (2016): 263-278. https://doi.org/10.1016/j.enconman.2016.05.083

[13] Jia, Yuting, Fengming Ran, Chuqiao Zhu, and Guiyin Fang. "Numerical analysis of photovoltaic-thermal collector using nanofluid as a coolant." *Solar Energy* 196 (2020): 625-636. https://doi.org/10.1016/j.solener.2019.12.069

[14] Hosseinzadeh, Mohammad, Ali Salari, Mohammad Sardarabadi, and Mohammad Passandideh-Fard. "Optimization and parametric analysis of a nanofluid based photovoltaic thermal system: 3D numerical model with experimental validation." *Energy Conversion and Management* 160 (2018): 93-108. https://doi.org/10.1016/j.enconman.2018.01.006

[15] Oztop, Hakan F., A. Z. Sahin, Hakan Coşanay, and I. H. Sahin. "Three-dimensional computational analysis of performance improvement in a novel designed solar photovoltaic/thermal system by using hybrid nanofluids." *Renewable Energy* 210 (2023): 832-841. https://doi.org/10.1016/j.renene.2023.04.115

[16] Khan, Ajiv Alam, Mohd Danish, Saeed Rubaiee, and Syed Mohd Yahya. "Insight into the investigation of Fe3O4/SiO2 nanoparticles suspended aqueous nanofluids in hybrid photovoltaic/thermal system." *Cleaner Engineering and Technology* 11 (2022): 100572. https://doi.org/10.1016/j.clet.2022.100572

[17] Rosli, Mohd Afzanizam Mohd, Cheong Jing Rou, Nortazi Sanusi, Siti Nur Dini Noordin Saleem, Nurfarhana Salimen, Safarudin Gazali Herawan, Norli Abdullah, Avita Ayu Permanasari, Zainal Arifin, and Faridah Hussain. "Numerical investigation on using MWCNT/water nanofluids in photovoltaic thermal system (PVT)." *Journal of Advanced Research in Fluid Mechanics and Thermal Sciences* 99, no. 1 (2022): 35-57. https://doi.org/10.37934/arfmts.99.1.3557

[18] Hasan, Husam Abdulrasool, Ali Arif Hatem, Lamiaa Abdulredh Abd, Azher M. Abed, and Kamaruzzaman Sopian. "Numerical investigation of nanofluids comprising different metal oxide nanoparticles for cooling concentration photovoltaic thermal CPVT." *Cleaner Engineering and Technology* 10 (2022): 100543. https://doi.org/10.1016/j.clet.2022.100543

[19] Filipović, Petar, Damir Dović, Ivan Horvat, and Borjan Ranilović. "Evaluation of a novel polymer solar collector using numerical and experimental methods." *Energy* 284 (2023): 128558. https://doi.org/10.1016/j.energy.2023.128558

[20] Rosli, Mohd Afzanizam Mohd, Irfan Alias Farhan Latif, Muhammad Zaid Nawam, Mohd Noor Asril Saadun, Hasila Jarimi, Mohd Khairul Anuar Sharif, and Sulaiman Ali. "A simulation study on temperature uniformity of photovoltaic thermal using computational fluid dynamics." *Journal of Advanced Research in Fluid Mechanics and Thermal Sciences* 82, no. 1 (2021): 21-38. https://doi.org/10.37934/arfmts.82.1.2138

[21] Rosli, Mohd Afzanizam Mohd, Irfan Alias Farhan Latif, Muhammad Zaid Nawam, Mohd Noor Asril Saadun, Hasila Jarimi, Mohd Khairul Anuar Sharif, and Sulaiman Ali. "A simulation study on temperature uniformity of photovoltaic thermal using computational fluid dynamics." *Journal of Advanced Research in Fluid Mechanics and Thermal Sciences* 82, no. 1 (2021): 21-38. https://doi.org/10.37934/arfmts.91.2.106119

[22] Aste, Niccolò, Claudio Del Pero, and Fabrizio Leonforte. "Thermal-electrical optimization of the configuration a liquid PVT collector." *Energy Procedia* 30 (2012): 1-7. https://doi.org/10.1016/j.egypro.2012.11.002

[23] Kell, George S. "Density, thermal expansivity, and compressibility of liquid water from 0. deg. to 150. deg.. Correlations and tables for atmospheric pressure and saturation reviewed and expressed on 1968 temperature scale." *Journal of Chemical and Engineering data* 20, no. 1 (1975): 97-105. https://doi.org/10.1021/je60064a005

[24] Hasan, Husam Abdulrasool, Ali Arif Hatem, Lamiaa Abdulredh Abd, Azher M. Abed, and Kamaruzzaman Sopian. "Numerical investigation of nanofluids comprising different metal oxide nanoparticles for cooling concentration photovoltaic thermal CPVT." *Cleaner Engineering and Technology* 10 (2022): 100543. https://doi.org/10.1016/j.clet.2022.100543

[25] Mishra, Purna Chandra, Sayantan Mukherjee, Santosh Kumar Nayak, and Arabind Panda. "A brief review on viscosity of nanofluids." *International nano letters* 4 (2014): 109-120. https://doi.org/10.1007/s40089-014-0126-3

[26] Rosli, Mohd Afzanizam Mohd, Yew Wai Loon, Muhammad Zaid Nawam, Suhaimi Misha, Aiman Roslizar, Faridah Hussain, Nurfaizey Abdul Hamid, Zainal Arifin, and Safarudin Gazali Herawan. "Validation Study of Photovoltaic Thermal Nanofluid Based Coolant Using Computational Fluid Dynamics Approach." *CFD Letters* 13, no. 3 (2021): 58-71. https://doi.org/10.37934/cfdl.13.3.5871

[27] Mishra, Purna Chandra, Sayantan Mukherjee, Santosh Kumar Nayak, and Arabind Panda. "A brief review on viscosity of nanofluids." *International nano letters* 4 (2014): 109-120. https://doi.org/10.1007/s40089-014-0126-3

[28] Xuan, Yimin, Qiang Li, and Weifeng Hu. "Aggregation structure and thermal conductivity of nanofluids." *AIChE Journal* 49, no. 4 (2003): 1038-1043. https://doi.org/10.1002/aic.690490420

[29] Seyf, Hamid Reza, and Behrang Nikaaein. "Analysis of Brownian motion and particle size effects on the thermal behavior and cooling performance of microchannel heat sinks." *International Journal of Thermal Sciences* 58 (2012): 36-44. https://doi.org/10.1016/j.ijthermalsci.2012.02.022

[30] Kakaç, Sadik, and Anchasa Pramuanjaroenkij. "Review of convective heat transfer enhancement with nanofluids." *International journal of heat and mass transfer* 52, no. 13-14 (2009): 3187-3196. https://doi.org/10.1016/j.ijheatmasstransfer.2009.02.006

[31] Katz, Aaron, and Venkateswaran Sankaran. "Mesh quality effects on the accuracy of CFD solutions on unstructured meshes." *Journal of Computational Physics* 230, no. 20 (2011): 7670-7686. https://doi.org/10.1016/j.jcp.2011.06.023